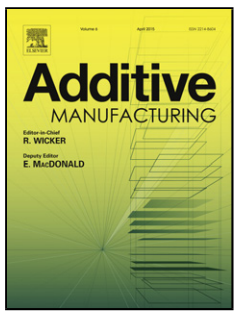

Title: 3-D printed composite microfluidic pump for wearable biomedical applications

Author: D.J. Thomas Z. Tehrani B. Redfearn

PII: S2214-8604(15)30004-X
DOI: http://dx.doi.org/doi:10.1016/j.addma.2015.12.004
Reference: ADDMA 59

To appear in:

Received date: 12-6-2015
Revised date: 14-11-2015
Accepted date: 14-12-2015

Please cite this article as: {http://dx.doi.org/

3-D Printed Composite Microfluidic Pump for Wearable Biomedical Applications

D.J. Thomas, Z Tehrani and B. Redfearn
College of Engineering, Swansea University, Bay Campus, Swansea
d.j.thomas@swansea.ac.uk +44 (0)1792 875533

Abstract

An integrated wearable 3-D printable microfluidic pump was developed, which uses a novel actuation process. Fused deposition manufacture 3-D printing was used as a means to accurately produce this device. This resulted in the fabrication of high precision integrated parts made from poly-lactic-acid bioplastic. By integrating an electro-magnetically actuated closed diffuser nozzle pump configuration a micro-fabricated microfluidic pump has been produced. Biofluids have been driven through the device by actuating a composite polydimethylsiloxane diaphragm actuated polymeric microstructure diaphragm membrane using electromagnetic force. This composite diaphragm was made by suspending 10μm iron particles in the polydimethylsiloxane at concentrations of 30%, 40% and 50%. It is shown that this device acts as an effective electromagnetic force actuated a pump. It is successfully demonstrated that a square wave electromagnetic signal is effective for generating a 2.2μL/min flow rate of biofluid. The integration of 3D printed devices to form a micropump is proven through practical testing which demonstrate a controllable flow rate was generated.

Keywords: 3D printing, Micropump, Bioplastic, Poly lactic acid polymers.

1. Introduction

Micropumps are an essential component in the development of a biomedical system to provide a mechanism to transport specific volumes of liquid [1-2]. They are crucial components for lab-on-a-chip-based, point of care (POC) devices, as they enable the transport of small and precise volumes of liquid through the system. There are several designs of micropump available for use, both mechanical and non-mechanical [3-4]. The majority of micropumps are membrane-based mechanical pumps [5-7], which work using a membrane that is actuated to increase or decrease the pressure in a chamber. The fluid then flows from an inlet through the chamber to an outlet, using either valves or a valveless microfluidic system to control the direction of flow.

Membrane-based micropumps can be categorised by their actuation method; Piezoelectric [8], Thermo-Pneumatic [9], Osmotic [10] and Magnetic [3,7,11]. Valveless systems have several benefits, as they have fewer moving parts [12]; they also have scaling potential due to the limiting Reynolds number [13]. There are two main system types used for valveless micropumps, these include peristaltic pumps which induce flow through phasing of symmetrical actuators [14], and the diffuser nozzle micro channel configuration pumps [15-18] which work through flow being induced through diffusers and nozzles due to a pressure gradient.

The diffuser nozzle configuration is optimum for producing an integrated pump because it has a simple construction, while also providing a constant flow. This mechanism works as the fluid flows in through the diffuser in supply mode when there is a pressure drop in the chamber, created by the actuation of the membrane. The nozzle in pumping mode results in producing an increased pressure in the chamber. This is due to Bernoulli's equation and the conservation of energy [17] as shown in (Eq 1).

$$(P_{in}-P_{out}/\rho) + 1/2\,(V^2_{in}-V^2_{out}) = 0 \qquad \text{[Eq 1]}$$

During this study 3D printing has been investigated as a method to fabricate a novel electromagnetically actuated micropump. This device is beneficial as it offers sufficient membrane deflection at a low voltage. It is suitable for integration with numerous microfluidic-based technologies that require contact with a patient for a prolonged period of time.

During this research work an accurate 3D printing method has been developed to make a simplified microfluidic pump. This is coupled with the low level of backflow for a single pump cycle is an attractive option for moving mL volumes of liquid. The critical aspect of this work is that 3-D Printing is used to make a low cost biomedical micropump. The key advantages of this work are

1. Fused deposition 3D printing has been used successfully to produce an integrated working micropump;
2. Deposited PLA plastic has been determined as being a durable and a mechanically suitable material for manufacturing precise integrated components;
3. Through the use of 3D additive manufacturing narrow diffuser elements have been produced within the micropump resulting in a liquid flow rate of between 2.2 – 2.4μL min $^{-1}$ being pumped;
4. 3D additive manufacturing has been shown to produce working integrated components.

2. Experimental Methods

2.1. FE-PDMS Composite Membrane Fabrication

Membranes were formed using Fe powder suspended in a Polydimethylsiloxane (PDMS) polymer base. These were made using 30%, 40% and 50% concentration of Fe powder to PDMS by weight with a membrane thickness of 750μm. The polymer base was mixed creating a 1:10 ratio of curing agent to base, PDMS solution. Fe powder was added to the PDMS base in situ to create varying mixtures of percentage Fe powder to PDMS. The membranes were then left to cure and degas at room temperature for twenty-four hours, forming the Fe/PDMS membrane film. Uniform dispersion and complete encapsulation of Fe in the PDMS polymer is required in order to ensure the membrane responds predictably to an applied magnetic field.

A solenoid electromagnet was used for the purpose of actuation. The magnetic flux around a solenoid electromagnet [19-21] are proportional for a solenoid [22] and the field around the solenoid is proportional to the field in the centre [20]. Because the field increases at the centre of a solenoid the force on the membrane at the area of interest will increase. To actuate the pump membrane, a square wave voltage has been used. To provide this square wave voltage to the electromagnet at the required voltage and current; a power supply, function generator, mosfet, and capacitor were utilised.

A function generator was used to control the voltage on a MOSFET gate. The power supply was connected to the source of the MOSFET, and the magnetic field was produced from the drain of the MOSFET. A capacitor was added to provide a current surge with the on signal, this allows the greatest current, and therefore the strongest magnetic field to be acting when the membrane is furthest away from the electromagnet.

2.2. 3D Printing

During this research fused deposition manufacturing (FDM) processes was used to deposit Poly Lactic Acid (PLA) chemical formula $(C_3H_4O_2)n$ plastics filament to form the geometry of the pump. The mechanical properties of PLA filament are shown in **Table 1**.

A layer resolution of 100μm was used during the 3D printing process in order to ensure that the micropump was produced to the appropriate level of accuracy. The pre-processor used to generate Gcode was ReplicatorG 34 this allowed the process parameters as shown in **Table 2** to be changed and convert the 3D model into G-Code instructions for the 3D printer.

2.3. Characterisation

Surface micrographs were captured using a Leica optical light microscope. In order to record and quantify the surface properties, a Taylor–Hobson form 2 Talysurf was employed with scans being carried out across a two-dimensional surface area, providing an accurate representation of the surface roughness data parameters. The R_a parameter has been used to assess surface roughness which is the arithmetic mean of departures from the mean line. Scanning electron microscopy (SEM; Ultra-High Resolution FE-SEM S 4800, Hitachi) was carried out at 10kV acceleration voltage and a 9.8mA emission current. The SEM scan resolution was 640x480pixels. Computational Fluid Dynamics (CFD) simulations were carried out using AutoDesk Multiphysics 2013. A salt and ethanol solution was used in order to observe and monitor the flow of fluid through the pump. This solution was placed in a Petri dish on a calibrated digital scales and the mass change of water over a defined time was measured. This mass flow rate was then converted into a volume flow rate using the relation of $\rho=m/V$.

3. Results and Discussion

3.1. Design and 3D Printing of the Micropump

The micropump was designed to be 3D printed in the form of a top and bottom section. Material properties and 3D processing capabilities have been examined to demonstrate the effectiveness of this manufacturing process to produce an Fe-PDMS actuated composite membrane.

A desirable flow rate for the pump to be comparable to current competitor products is between 2 and 100 microlitres per minute **[9-10]**. The driving frequency of the electromagnet needs to be optimised to obtain the maximum flow rate **[14, 23]**. The micropump has an enclosed diffuser, chamber, Fe-PDMS membrane, bottom and the inlet and outlet tubes.

As shown in **Figure 1** is the design concept of the micropump which uses the Fe-PDMS composite membrane as a magnetically actuated microstructure. The pump design is operated periodically through the use of an electromagnet being pulsed on and off. This effects the Fe-PDMS diaphragm and causes it to displace, which forces more liquid through the outlet than back out through the inlet. This causes oscillation of the composite membrane, which compresses the pump chamber and generates fluid flow.
The pump was first designed to optimise the diffuser nozzle assembly that allows the pump to act without valves. 3D printing offers the ability to produce an integrated device with the diffusers accurately fabricated as shown in **Figure 2**. The effectiveness of a micropump is based upon the geometries of the inlet, outlet and chamber and the critical 10° value of the inlet valve. The main advantage of this method is the simplicity of device fabrication. This is coupled with the low level of backflow for a single pump cycle is an attractive option for moving mL volumes of liquid.

As shown in **Figure 3** is the white light surface profiles, these show that the top surfaces produced using 3D printing produced a higher degree of surface roughness than the sides. As measured, the 3D printing process produced a measured R_a of 7.64µm with a maximum with the sides having a much lower roughness of R_a 2.0µm. This suggested that the 3D Printing manufacturing method is capable of producing the required low surface roughness profiles. This reduces surface area and subsequently friction of the liquid through the device.

The 3D printed geometries of the diffusers produced are shown in **Figure 4.** Here the area ratio between the outlet and inlet is equal to 3.75. The length of the diffuser or nozzle in relation to the inlet is equal to 17. The depth of the diffuser or nozzle is arbitrary to the coefficient of performance and depends on the flow rate required this was made to be 400µm. The optimum ratio of dimension can be determined by looking for the values to gain the maximum coefficient of performance whilst not creating stall within the micropump.

As shown in **Figure 5** are the micrographs of the diffuser elements. It was observed that there is good degree of adhesion between the 3D printed layers and a non-porous solid finish is produced.
As **Figure 6** shows if the print travel speed is not at an optimum level then this can result in the formation of closed features. At 40mm sec^{-1} the deiffuser elements became closed and at a high print speed of 65mm sec^{-1} a discontinuous filament mesh was produced. Therefore, a print speed of 55mm sec^{-1} resulted in the generation the fine features necessary for producing the internal diffuser components.

Axonometric profiles of the 3-D Printed as shown in **Figure 7** show the striations produced on the surface that has an increased surface area. The layers produced are by deposition on top of each other, with the subsequent layers depended on the

ones produced before. Therefore, it is critical that the deposition of layers is controlled in such a way that the formation of surface inconsistencies is avoided.

3.2. Fabrication and Integration of Fe-PDMS Membrane

As shown in **Figure 8** are micrographs of the Fe-PDMS composite membranes produced using different concentrations of Fe. In order to ensure that are Fe particles are fully encapsulated in PDMS an extra 100μm layer of PDMS was made and used to cover the surface. This was to ensure that there an no particles were present on the surface which could react with the fluid inside. The membrane must deform sufficiently, in response to the applied magnetic field, so that the desired volume of liquid can be pumped by the actuation of the membrane. **Table 3** shows the deflection of the membranes when applied to deflect in reaction to a magnetic field. Measurements of the deflection of the different Fe-PDMS composites observed that the 40% ratio of Fe to PDMS has the greatest deflection. Since the Fe-PDMS can only be displaced in the direction of the actuating electromagnet, actuation is carried out towards the inside of the chamber.

750μm membranes can be flexed to the required deflection required in-order to generate the required momentum within the micropump. Using a concentration of Fe to PDMS of 40% achieves the correct balance between the stiffness of the material. This is coupled with the appropriate concentration of Fe in order to produce a required actuation response. At lower concentration of 30% Fe-PDMS then the flexibility is higher but there is lower concentration of Fe in order to react to the electromagnet and the opposite occurs at a concentration of 50%. As shown in **Figure 9** is the assembly process in which the micropump was built. The Fe-PDMS membrane is bonded to the surface of the 3D printed plastic, which maintains a tight seal. The key advantage of this manufacturing method and design over other diaphragm micropumps is that the device is simple to fabricate. It is also flat enough to be integrated with wearable medical devices.

As shown in **Figure 10** is the final assembly of the micropump with the electromagnet attached to its base. The electromagnet has been attached to a function generator in order to control the waveform used to simulate the pumping process.

3.3. Pump Performance

As the frequency was changed then the flow rate ($\mu L/min^{-1}$) also changes as shown in **Figure 11**. Between frequencies of 0.25 – 0.5Hz the flow rate remained stable at $2.2\mu L/min^{-1}$, however, as this was increased between 2 and 4Hz then there is slight drop of rate to $2.1\mu L/min^{-1}$. At frequencies above this it was noticed that bubbles were being produced from the inlet pipe. This resulted in an increased back flow. Here, although the pump is working at its maximum efficiency, the increased volume is results from an over extension of the membrane.

This is also a case that the membrane does not relax in time as the next square wave is being applied. This is an oscillation without the membrane moving back into its resting position. At a frequency of 10Hz then the pump is working inefficiently as a result the Fe-PDMS diaphragm cannot flex any further. This is due to the applied waveform being too fast and the volume flow rate reduces.

As shown in **Figure 12** during the first stroke this resulted in a first initial drop of liquid being expelled from the micropump as the pump settles into normal operation**.** Between different frequencies following the first few strokes the level of liquid expelled through the outlet this then remained stable. Therefore, after an initial period that the pump has an increase in flow rate this stabilised and remained constant. The frequency was then adjustable in order to control the flow rate. In order to test the flow on liquid through and to test for leakage, salt crystals were suspended in ethanol and this solution. This was then passed through the micropump at a 2Hz frequency as **Figure. 13** shows.

As salt crystals were observed under the microscope to observe flow and disruption in the flow rather than lateral motion be generated. Under a low pressure liquid flow rate of 2.2μL/min this resulted in a momentum of approximately 0.25mm/sec through the outlet with no turbulence outside the device.

3.4. Computational Fluid Dynamics Analysis

Computational fluid dynamics (CFD) of the micropump revealed the complex fluid flow properties through the structure. As shown in **Figure 14** is a section though the micropump which shows the change in velocity of the liquid through the micropump inlet and outlet valves. One of the main features of the device is that there is a small induced level of backflow. However, there is a momentum generated to allow a working pump mechanism. The decrease in cross sections area (CSA) between the different regions of the micropump causes an increase in the velocity.

As shown in **Figure 15** are flow simulations of the movement of liquid through the device in which there is a 50mm sec^{-1} movement of the liquid as it enters the constricted part of the nozzle.

The flow behaviour of liquid results in a movement around the outside of the pump chamber. During the start of the stroke, liquid is forced around the outside of the chamber and through the outlet. This movement of flow around the chamber suggests that there is no stagnation of fluid because of the continuous momentum around and out of the chamber. Overall, rather than a smooth flow there is a pulsing mode of fluid displacement in which after the initial burst of liquid this moves as a wave and through the outlet.

4. Conclusions

This research demonstrates that 3D printing can be used to accurately fabricate integrated devices. An electromagnetic actuation of a Fe-PDMS membrane valveless micropump is a viable proposal for use in microfluidic liquid transfer. It was found that the electromagnetic actuation, with an optimised pump configuration and build procedure gained a comparable flow rate of 2.2mL min^{-1}.

By adjusting the pulse frequency then the flow rate of between 2.2 and 2.4μL min^{-1} could be achieved and was controllable. Therefore this microfluidic pump has a controllable flow rate. It was found that an Fe-PDMS membrane made with a 40% mix by weight of Fe to PDMS with a 750μm thickness created the most actuation movement within the pump.

This micropump technology has been proven through practical testing demonstrates a flow rate that is useful for integration with point of care drug delivery devices for healthcare applications. The performance of the diffuser/nozzle valving principle critically depends on the precise geometries of the diffuser/nozzle elements being 3D Printed. The 3D printed diffuser/nozzle elements has the precise and controlled features produced for a reliable and predictable operation.

Acknowledgements

The authors would like to thank the support of Swansea Universities Centre for NanoHealth during the pursuit of this research.

References

1. Pumera M, Sánchez S, Ichinose I, Tang J. Electrochemical nanobiosensors. Sensors and Actuators B: Chemical. 2007 5/21/;123(2):1195-205.

2. Wang C-H, Lee G-B. Automatic bio-sampling chips integrated with micro-pumps and micro-valves for disease detection. Biosensors and Bioelectronics. 2005 9/15/;21(3):419-25.

3. Al-Halhouli AT, Kilani MI, Buettgenbach S. Development of a novel electromagnetic pump for biomedical applications. Sensors and Actuators a-Physical. 2010 Aug;162(2):172-6.

4. Zhao YJSaTS. Modelling and test of a thermally-driven phase-change nonmechanical micropump. Journal of Micromechanics and Microengineering. 2001;11(6):713.

5. Gerlach T, Wurmus H, editors. Working principle and performance of the dynamic micropump. Micro Electro Mechanical Systems, 1995, MEMS '95, Proceedings IEEE; 1995 29 Jan-2 Feb 1995.

6. Hopt FGaADaMHaPWaH-JSaUT. A generic analytical model for micro-diaphragm pumps with active valves. Journal of Micromechanics and Microengineering. 2005;15(4):673.

7. Nagel JJ, Mikhail G, Hongseok Moses Noh, Koo J. Magnetically actuated micropumps using an Fe-PDMS composite membrane. International Society for Optical Engineering. 2006.

8. Cui Q, Liu C, Zha X. Study on a piezoelectric micropump for the controlled drug delivery system. Microfluidics and Nanofluidics. 2007 2007/08/01;3(4):377-90.

9. Mousoulis C, Ochoa M, Papageorgiou D, Ziaie B. A Skin-Contact-Actuated Micropump for Transdermal Drug Delivery. Biomedical Engineering, IEEE Transactions on. 2011;58(5):1492-8.

10. Stevenson CL, Santini Jr JT, Langer R. Reservoir-based drug delivery systems utilizing microtechnology. Advanced Drug Delivery Reviews. 2012 11//;64(14):1590-602.

11. Tzong-Shyng L, Pin-Chin J, editors. Fe-PDMS fabricated microchannels for peristaltic pump applications. Nano/Micro Engineered and Molecular Systems (NEMS), 2010 5th IEEE International Conference on; 2010 20-23 Jan. 2010.

12. Andersson H, van der Wijngaart W, Nilsson P, Enoksson P, Stemme G. A valve-less diffuser micropump for microfluidic analytical systems. Sensors and Actuators B: Chemical. 2001 2/10/;72(3):259-65.

13. Jensen PGaJBaOS. Microfluidics-a review. Journal of Micromechanics and Microengineering. 1993;3(4):168.

14. Berg JM, Anderson R, Anaya M, Lahlouh B, Holtz M, Dallas T. A two-stage discrete peristaltic micropump. Sensors and Actuators a-Physical. 2003 Mar 15;104(1):6-10.

15. Jiang XN, Zhou ZY, Huang XY, Li Y, Yang Y, Liu CY. Micronozzle/diffuser flow and its application in micro valveless pumps. Sensors and Actuators a-Physical. 1998 Oct 1;70(1-2):81-7.

16. Jiang Dan and Li S-J. The dynamic characteristics of a valve-less micropump. Chinese Physics B. 2012;21(7):074701.

17. R HJ, O BR. Fundamentals of Engineering Thermodynamics second edition. Singapore: McGraw Hill; 1992.

18. Cheng Y-L, Lin J-H. Manufacture of three-dimensional valveless micropump. Journal of Materials Processing Technology. 2007 Oct 1;192:229-36.

19. University C. Why are some materials magnetic? [Internet] 2013 [cited 2013 23/04/13]; Available from: http://www.doitpoms.ac.uk/tlplib/ferromagnetic/why_magnetic.php.

20. Jiles D. Introduction to magnetism and magnetic materials. London: Chapman & Hall; 1991.

21. Vogel O, Ulm J. Theory of proportional Solenoids and Magnetic Force Calculation Using COMSOL Multiphysics. COMSOL Conference; Stuttgart2012.

22. Griffiths DJ. Introduction to Electrodynamics. In: Kim D, editor. 3 ed. San Fransisco2008. p. 269-73.

23. Nguyen N-T, Meng AH, Black J, White RM. Integrated flow sensor for in situ measurement and control of acoustic streaming in flexural plate wave micropumps. Sensors and Actuators A Physical. 2000;79(2):115.

24. L MR. Applied Fluid Mechanics. 6 ed. Jurong Singapore: Prentice Hall; 2006.

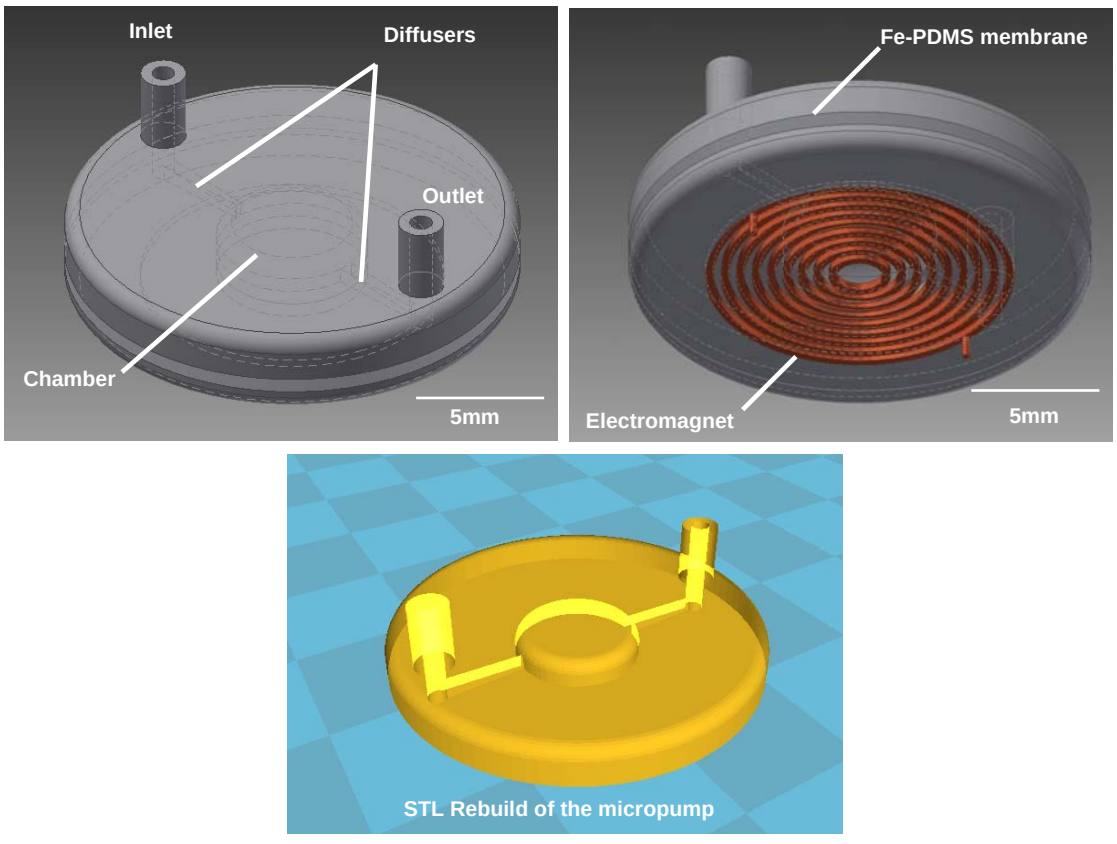

Figure. 1. Principle of the design for the electromagnetically actuated microfluidic pump and the critical dimensions of the 3D Printed components.

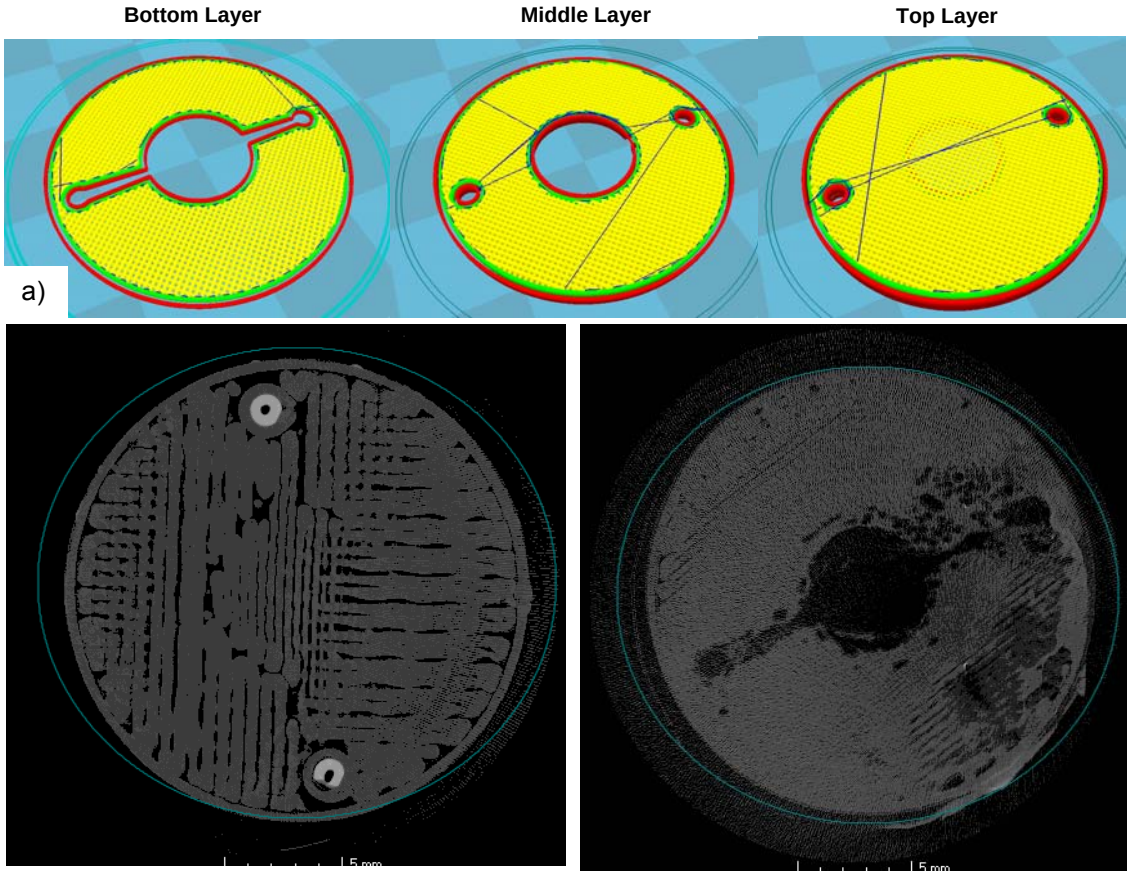

b)

Figure. 2. (a) Slicer engine rebuild of the microfluidic pump, and (b) cross sectional scans through the device.

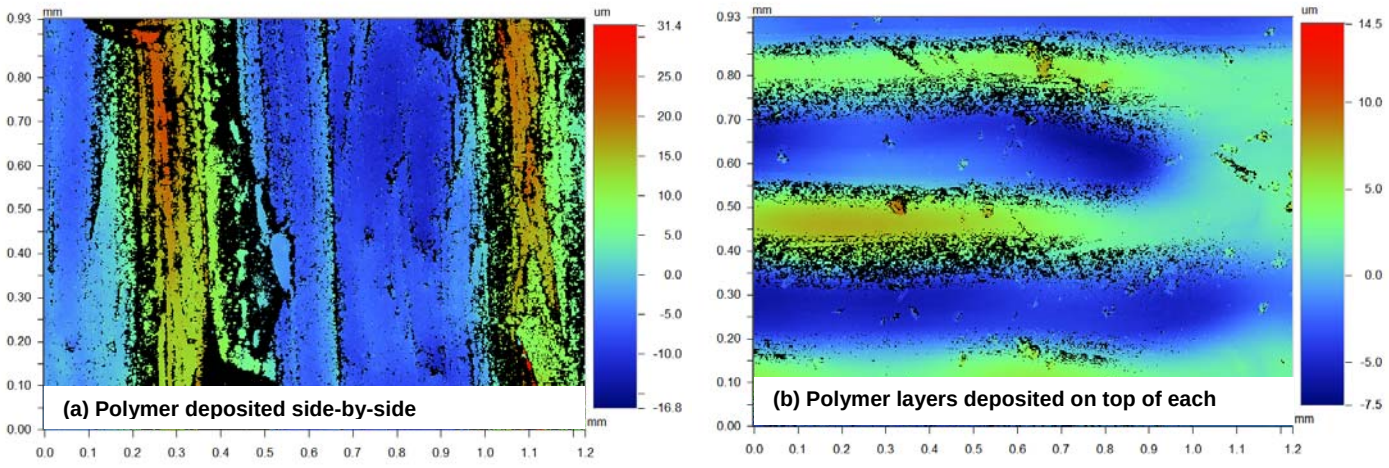

Figure 3. White light interferometer profiles of (a) top 3D Printed top surface and (b) side view showing the layer-by-layer pattern produced.

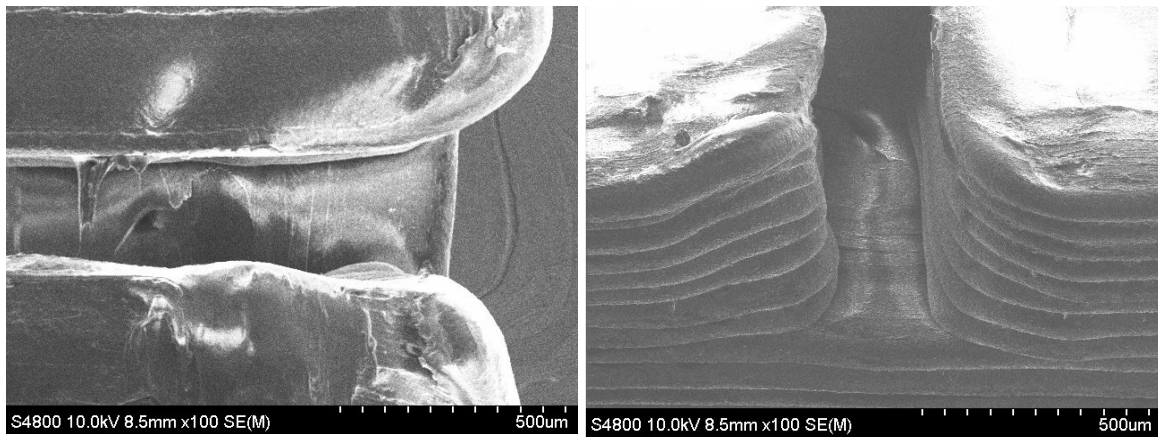

Figure. 4. Micrographs taken of the 3D printed diffuser assembly.

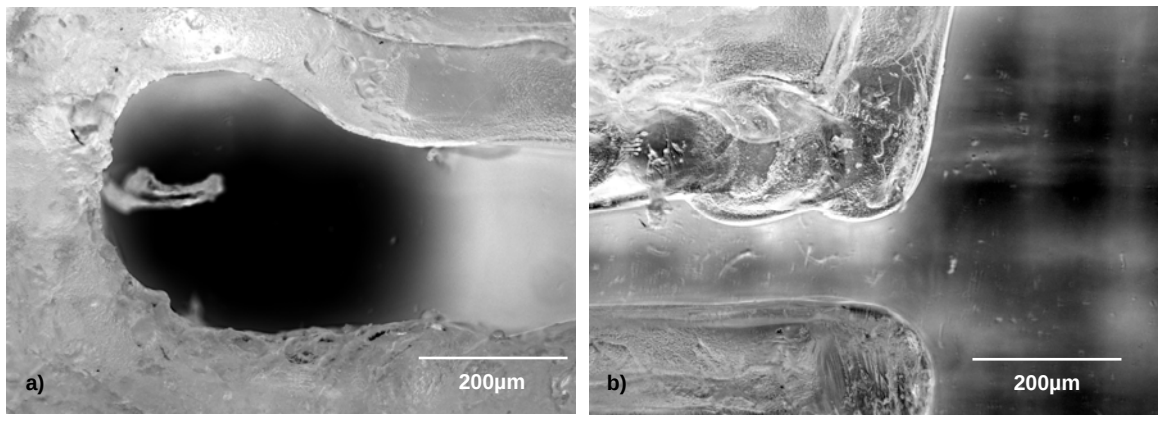

Figure 5. Micrographs of the 3-D Printed diffusers (a) inlet diffuser from the inlet pipe and (b) outlet into the chamber

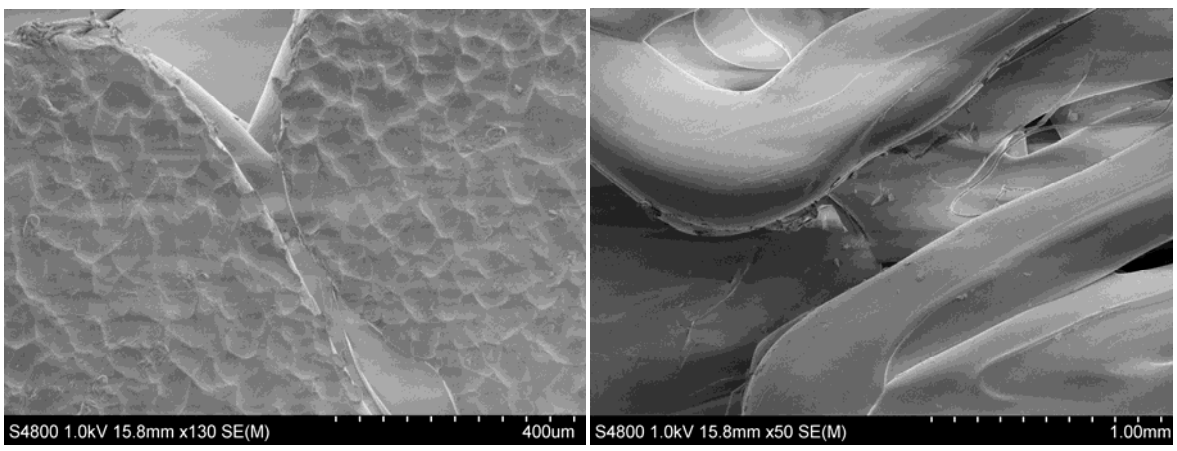

Travel speed 40mm sec^{-1} Travel speed 65mm sec^{-1}

Figure. 6. Scanning electron micrographs of the 3D printed surfaces produced at different deposition speeds.

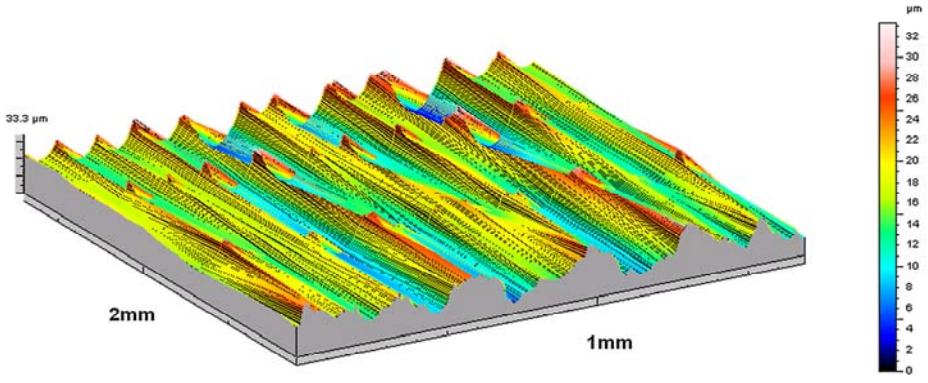

Figure 7. 3-D Axonometric white light surface profile of the surface layer produced on the side wall of the micropump chamber.

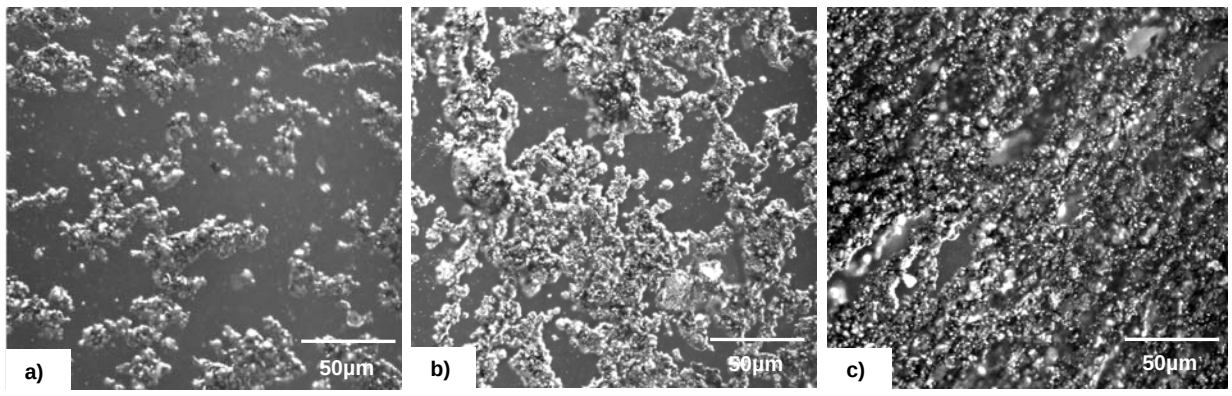

Figure 8. Micrographs of Fe-PDMS membrane at (a) 30% (b) 40% (c) 50% concentrations of Fe by weight.

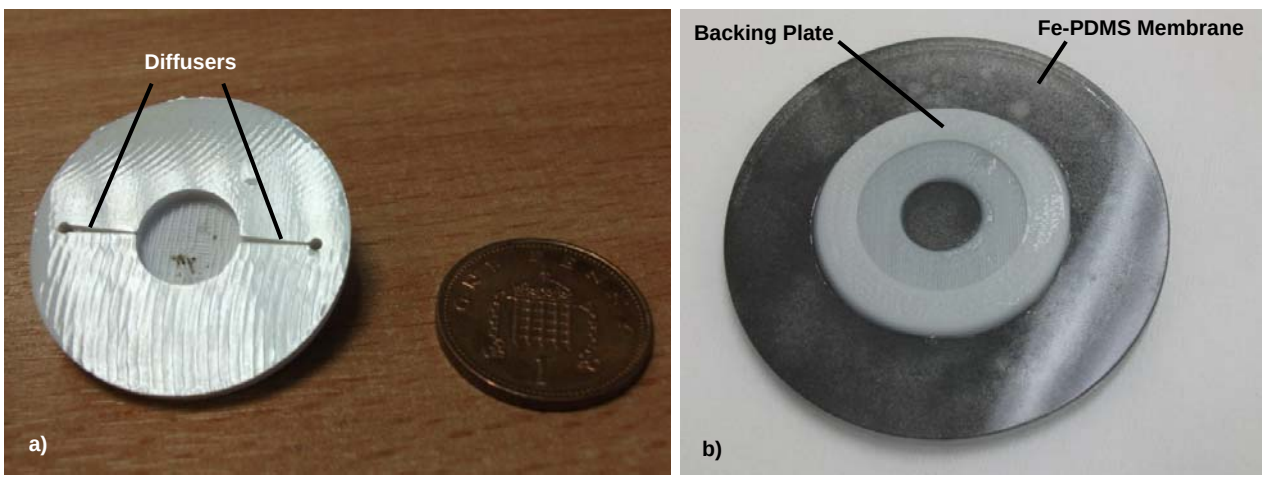

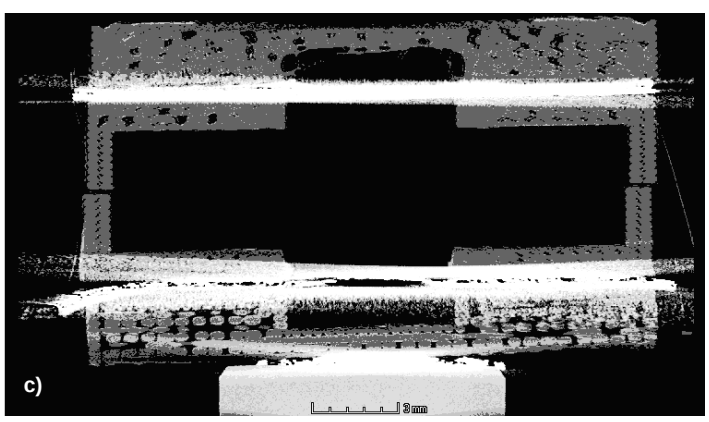

Figure 9. Assembly of the micropump (a) micropump with integrated diffusers and chamber (b) integration with Fe-PDMS membrane and (c) x-ray scan through the assembly.

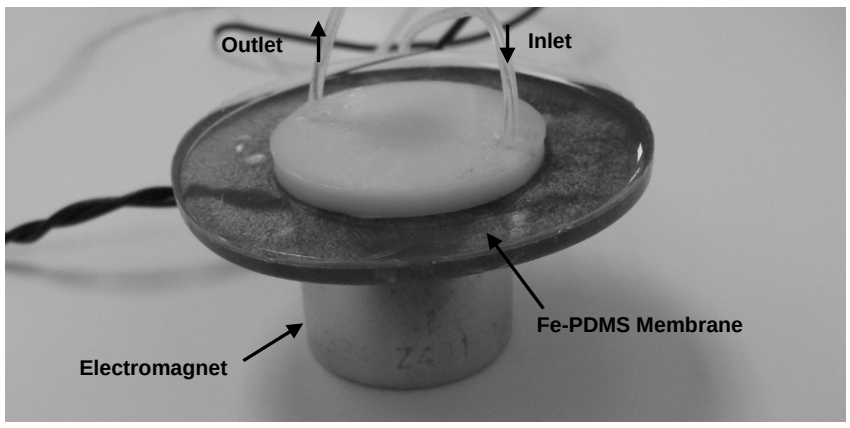

Figure 10. Final assembly of the micropump with integration of an electromagnetic actuator.

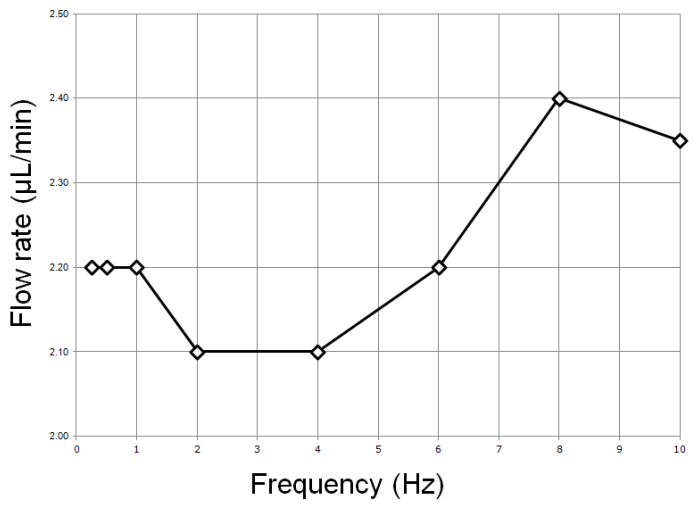

Figure 11. Volume flow rate at in µL/min at frequencies between 0.25Hz and 10Hz.

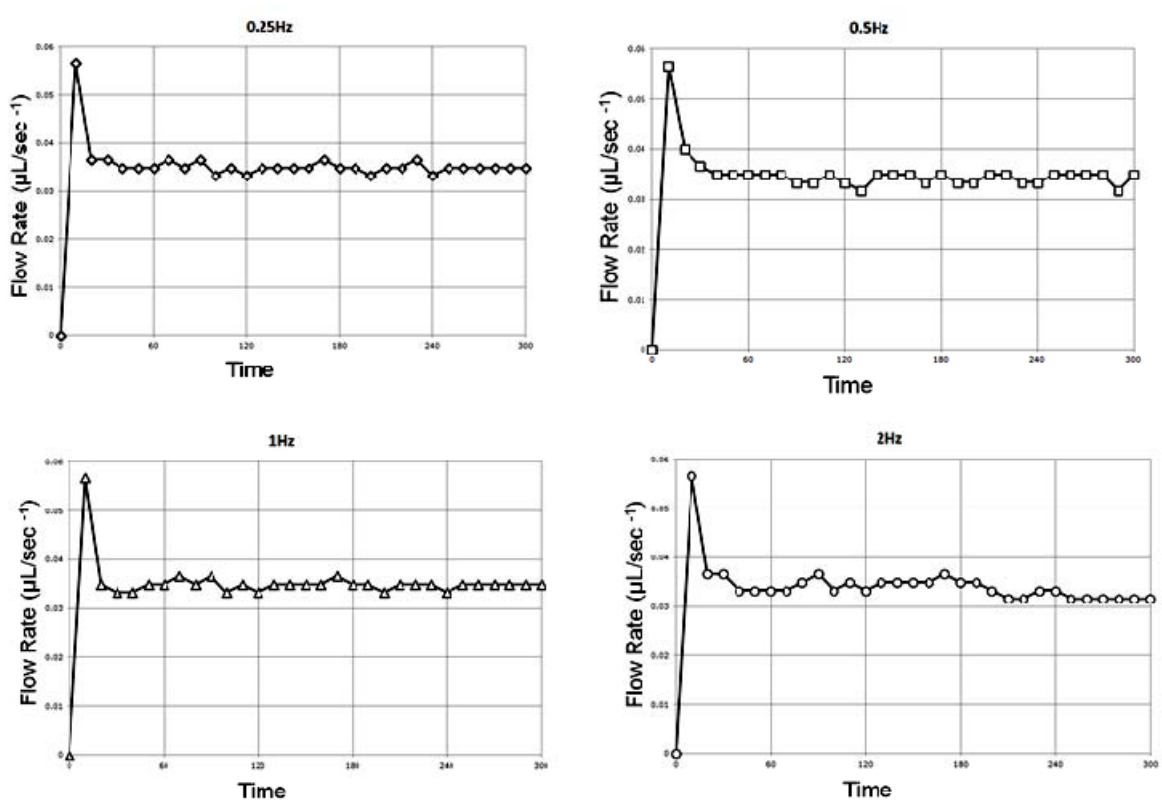

Figure 12. Flow rate (µL/sec) of the pump throughout using 0.25Hz, 0.5Hz, 1Hz and 2Hz frequencies.

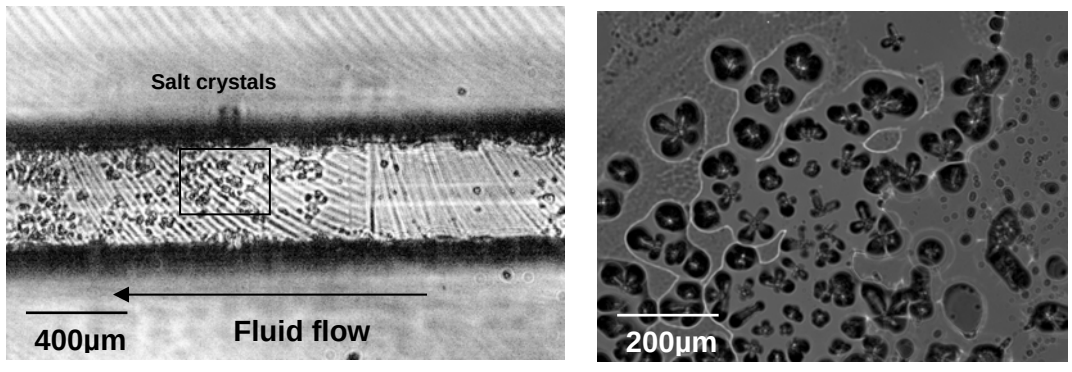

Figure.13. Flow of liquid ethanol with one molar sodium chloride crystals used to observe the flow of liquid.

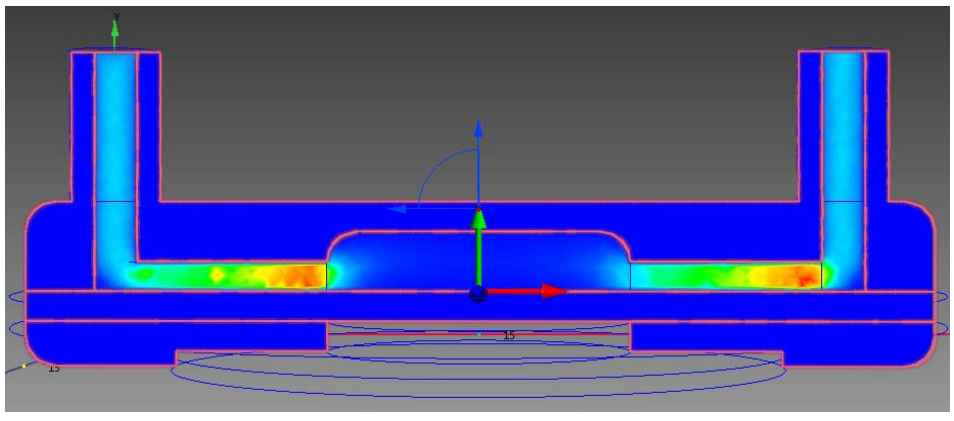

Figure. 14. Computational fluid dynamics of the flow of liquid through the micropump inlet and outlet diffusers.

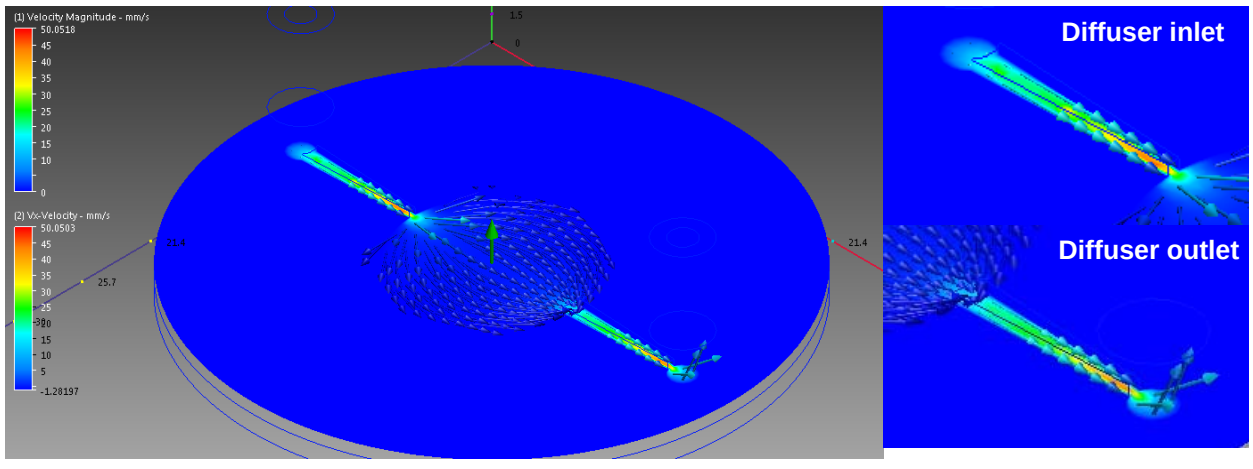

Figure. 15. Computational fluid dynamics of the flow of liquid through the chamber at the start of a stroke.

Table. 1. Mechanical properties of 3D printed PLA plastic.

Tensile Strength	Yield Strength	Elongation	Youngs Modulus	Glass Transition Temperature (Tg)	Specific Gravity
53MPa	44MPa	2.5%	3.2GPa	65°C	1.25

Table. 2. Process parameters as applied using the software environment used for 3D printing PLA plastic.

Parameter	Process Settings
Object Infill	100%
Layer height	100μm
Number of shells	2
Travel Rate	55mm sec^{-1}
Plastic filament diameter	1.75mm
Extruder outlet diameter	400μm
Extrusion temperature	230°C
Build plate temperature	50°C

Table 3. Deflections for different compositions of FE-PDMS membranes.

Fe content (wt%)	Membrane Thickness (μm)	Deflection (mm)
30%	750	0.45
40%	750	2.25
50%	750	1.85